Design and Implementation of CCNY DC Microgrid Testbed

Mahmoud Saleh, *Student Member, IEEE*, Yusef Esa, *Student Member, IEEE*, Yassine Mhandi, *Student Member, IEEE*, Werner Brandauer and Ahmed Mohamed, *Member, IEEE*

***Abstract*—This paper presents the design, control, energy management, and implementation of the City College of New York (CCNY) direct current (DC) microgrid laboratory testbed. This facility was custom designed and implemented by researchers at CCNY with minimal off-the-shelf components to enable significant flexibility and reconfiguration capability. The microgrid consists of renewable energy resources, energy storage system and controllable loads, and can operate in either a grid-connected or an islanded mode. The design steps, requirements, and results of the developed testbed were discussed. Moreover, several operational scenarios were tested. The experimental results verify the applicability and flexibility of the developed microgrid testbed.**

***Index Terms*—CCNY, control, DC-DC converters, distributed energy resources, inverters, microgrid.**

I. Introduction

Electric power systems have been designed and engineered to be highly reliable; the frequency and duration of power outages are low as compared to other engineering systems of a comparable complexity, e.g. the cellular communication system. However, there is a national call for increasing the grid resiliency, and self-healing capability. Compared to the legacy power grid, a resilient grid is less likely to fail, and more importantly, if it is to fail due to low-probability high-impact events, such as natural disasters, cyber-attacks and human errors, it shall be able to partially sustain the power supply, and restore the service faster and more flexibly. The imperative to make the power system more resilient, along with other objectives, led to the introduction of smart grid, with a major role expected to be played by renewable energy based microgrids [1-3].

According to the U.S. Department of Energy, "A microgrid is a group of interconnected loads and distributed energy resources within clearly defined electrical boundaries that acts as a single controllable entity with respect to the grid and that connects and disconnects from such grid to enable it to operate in both grid-connected or island mode" [4]. Consequently, the design and control of microgrids have received significant attention lately [5-8].

Operation of microgrids proposes several advantages to customers and utilities including improved energy efficiency, facilitated renewable energy and electric vehicle integration, improved voltage control and security of supply [9]. There are two main types of microgrids, namely AC and DC microgrids. In AC microgrids, the various resources and loads are interfaced through a common AC bus. Designing and operating an AC microgrid is relatively easily, since it builds upon our understanding of the legacy AC power network. However, as compared to DC microgrid, AC microgrid is less efficient due to the losses associated with the power electronic converters required to interface renewable energy resources, energy storage systems and DC loads [8, 9].

On the other hand, in DC microgrids, the common bus is DC [10-12]. Therefore, synchronization with the utility grid is not required for the individual microgrid assets. It is more efficient than AC microgrids, it encounters no power factor losses and it is more hospitable to increased renewable energy penetration levels. The major challenges associated with DC microgrids are to design an effective protection system, due to the absence of a zero crossing point, and to maintain their stability under heavy disturbances, especially if the microgrid converters are tightly regulated. In this paper, we will focus on DC microgrids.

Even though research results in the literature have addressed many of the technical challenges that present stumbling blocks against wide-scale deployment of microgrids, there is a wide gap between the research outcomes and their actual implementation. A major reason for this, in our view, is the lack of testing platforms where practical limitations, theories and simulation results can be credibly verified. Microgrid testbeds are essential tools to perform research on microgrids in grid-tied and islanded modes.

There are challenges associated with implementing microgrids, e.g. designing an optimal control and monitoring architecture. Some of the research that has been performed to address those challenges was tested on purely software-based simulations [13-16]. Other articles have suggested to build a hardware-in-the-loop (HIL) microgrid testbed [17]. This testbed did not depend on hardware, but rather heavily depended on software simulations since, according to the authors of [17], fixed hardware configuration is time consuming and costly to reconfigure. Some researchers designed a hardware-based microgrid testbed, but using off-the-shelf components [18, 19]. Moreover, most of the effort to develop microgrid testbeds in the literature was directed towards AC microgrids.

In this paper, we will present a completely flexible and controllable DC microgrid testbed, which has been designed and implemented at the City College of New York. The developed DC microgrid was custom designed with minimal off-the-shelf components, to give us a high level of flexibility in reconfiguring the hardware setup to test various ideas and

concepts. The focus of the paper will be on the design of the testbed, including some case studies that highlight some of the capabilities of the microgrid testbed. The purpose of the paper is to share our observations and design considerations with the research community, especially to those who may be interested in reproducing a similar facility.

The rest of the paper will be organized as follows: in section II, the structure of the developed DC microgrid testbed will be presented; in section III, the system controllers will be described; in section IV, the design of the various components will be summarized; in section V, experimental results will be presented and discussed; finally in section VI, the main conclusions of the study will be listed.

II. CCNY DC Microgrid Structure and Hardware Architecture

Simplified block and circuit diagrams for the developed testbed are illustrated in Figs. 1 and 2. The microgrid is connected to the utility grid (i.e. the three-phase 208 V legacy grid) via a Solid State Relay (SSR), which enables the microgrid to tie to the grid or island itself when needed. The testbed was structured using the following main components:

- Two 6 kW programmable power supplies, which can be programmed to emulate photovoltaic profiles, or correspond to a pre-defined power-time curve. The power supplies were from Magna-Power, model: XR600-9.9/2008+HS programmable DC power supply-photovoltaic power profile emulator.
- Two dSPACE real-time digital control boards, using RTI 1104 platform.
- Two 12 kW full bridge IGBT modules by SEMIKRON, model: Semistack.
- A custom designed 10 kW DC-DC boost converter, to interface distributed energy resources (DER).
- A custom designed 10 kW DC-DC bidirectional converter, to interface the battery and control its charging and discharging.
- Interface and protection circuits, and filters.
- Several custom designed metering systems utilizing (voltage transducer (VT): LV25-NP by LEM, and current transducer (CT): LA25-NP by LEM).
- A custom designed AC/DC static/dynamic load emulation system that offers a controlled variable load, with a maximum of 6 kVA for AC load, and 10 kW for DC load.
- A CCNY-Energy institute 1.4 kW flow batteries composed of 16 cells.

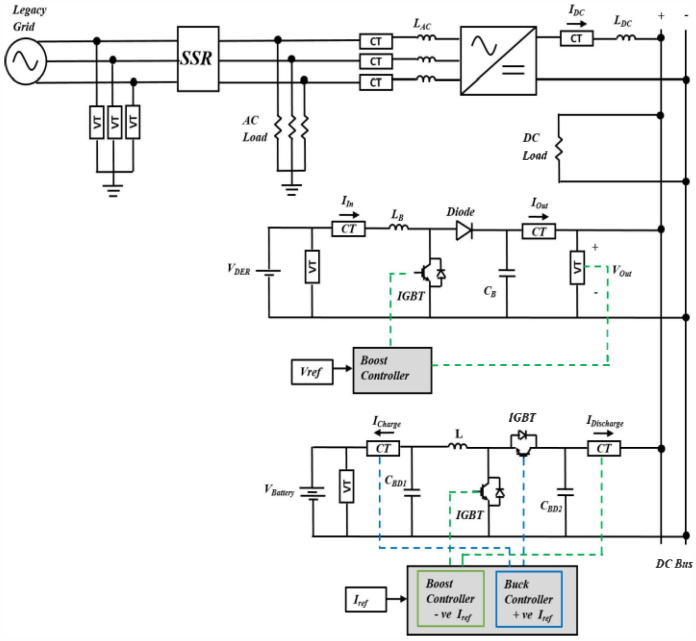

Fig. 2. Simplified circuit diagram of the CCNY DC Microgrid testbed.

As shown in Fig. 2, the AC load (realized by the developed load emulator) is shared between the utility grid and the CCNY DC microgrid through the AC bus, which is monitored by the implemented metering system (VTs and CTs). The filter is being used to reject harmonics of the inverter current, in the

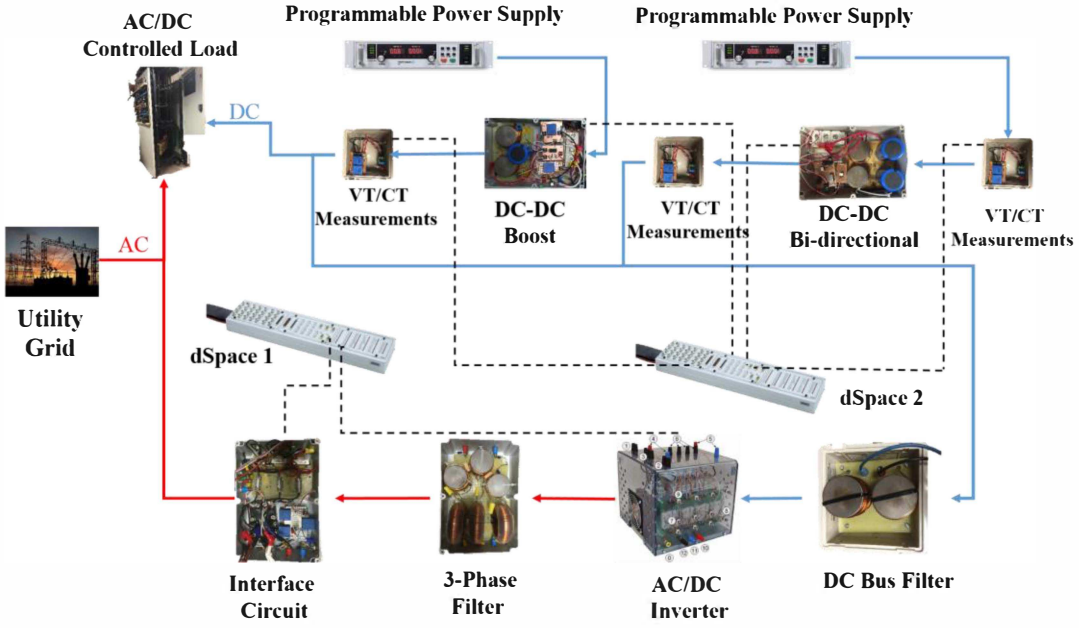

Fig. 1. Block diagram for the CCNY Microgrid testbed.

grid-tied mode. The SSR is located at the point of common coupling (PCC) to grid-tie or island the microgrid based on a pre-defined algorithm and islanding detection mechanism. On the DC side, the DC bus links the DC dynamic load, the batteries through the bidirectional DC/DC converter, the photovoltaic emulator through a DC/DC boost converter and the Inverter through an LC filter to reduce the voltage/current ripples.

The MATLAB/SIMULIK based state machine control was implemented on two dSPACE units to act as an Energy Management System (EMS). The main dSPACE was utilized to perform as a Microgrd Central Controller (MGCC), which manages the power exchange with the main grid in a grid-tied mode, among other functions. For instance, it relays set points to the various converters within the microgrid. A second dSPACE acts as a local controller for the DERs connected to the DC bus.

III. System Controllers

A. DC-DC boost converter controller

DERs output is typically intermittent by nature, e.g. due to cloud variations in the case of photovoltaic systems. Therefore, a controlled DC-DC boost converter is needed to regulate the output voltage and/or track the maximum power point. A PI controller was used with K_p and K_i values of 0.002 and 0.2, respectively. One of the main features of the developed DC microgrid is flexibility. The controller parameters can be easily changed, e.g. the value of K_i can be changed to decrease the rise time and give a quick response to operating point variations, on the expense of introducing higher overshoot.

B. DC-DC bidirectional converter controller

Stationary storage devices require bidirectional DC-DC interface to control their charging and discharging processes. We developed a converter that operates between two fixed voltages, the DC bus voltage and the battery system voltage. Two PI controllers were implemented to achieve a desired reference current signal, with K_p and K_i equal to 0.02 and 110, respectively, in the charging mode, and K_P and K_i of 0.02 and 3, respectively, in case of discharging. The battery charger controller can correspond to a power/current reference signal for charging and discharging, or can regulate the DC bus voltage if needed, in case of an islanded microgrid.

C. Inverter controller

A bidirectional AC/DC converter was used to control the amount of active and reactive power exchanged with the main grid. A robust controller was implemented to synchronize with the utility grid and seamlessly send or receive active or reactive power when demanded.

Fig. 3 presents a block diagram for the control system of the converter. v_{abc} is measured from the utility grid side to acquire the phase and frequency using a phase locked loop (PLL), to enable synchronization with the grid. The inverter output currents in the abc frame of references are converted to dqo frame of references, and regulated through PI controllers to generate the dq voltages, which are used to generate the modulation signals [20, 21].

IV. Validation, Customization and Testing of Individual Interfaces

A. DC-DC Boost converter:

The topology of the DC-DC converter was customized and designed to boost fluctuated or variable input voltage (V_{in}) in the range of 100 V-300 V up to a higher constant DC output voltage (V_{out}) of 300 V-400 V, which represents the voltage level of the DC bus, with ripple less than 5 V, which is tolerable for the used capacitor [22]. To maintain the microgrid stability, the inductance and capacitance were selected higher than the critical values described by [23]:

$$L_c = \frac{D(1-D)}{2f} R \quad (1)$$

$$C_c = \frac{D}{2fR} \quad (2)$$

Where L_c is the critical value for inductance to maintain the continuous inductor current, C_c is the critical value for the capacitance to maintain continuous capacitor voltage, D is the large-signal duty cycle, f is the switching frequency and R is the load resistance. The worst case scenario was assumed, when the maximum load R = 100 ohms. The switching frequency f was set to 5 kHz to avoid audible noise and high-frequency parasitic elements. Fig. 4 shows L_c versus the duty cycle. Inspecting (1), we can find the threshold for the inductance for continuous mode to be D = 0.5.

The IGBTs/diodes voltage ratings were selected such that when the IGBT is open, it is subjected to V_{out}. Because of the usual double voltage switching transients, the IGBT was rated to $2\times V_{out}$. When the IGBT is closed, the diode is subject to V_{out}. The diode was conservatively rated to $2\times V_{out}$ as well [24].

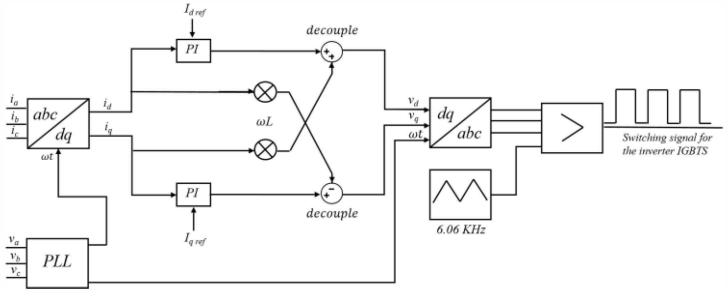

Fig. 3. Control diagram of active and reactive current control of the inverter.

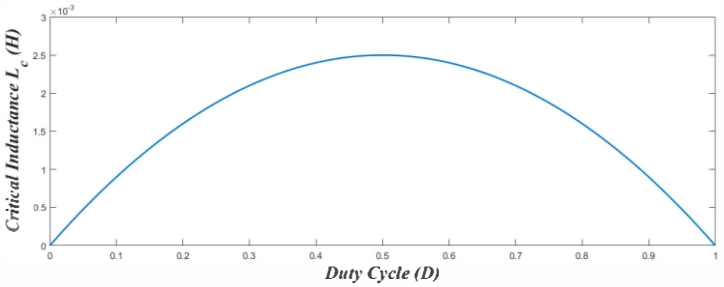

Fig. 4. L_c versus duty cycle at: R = 100 ohms and f = 5 kHz.

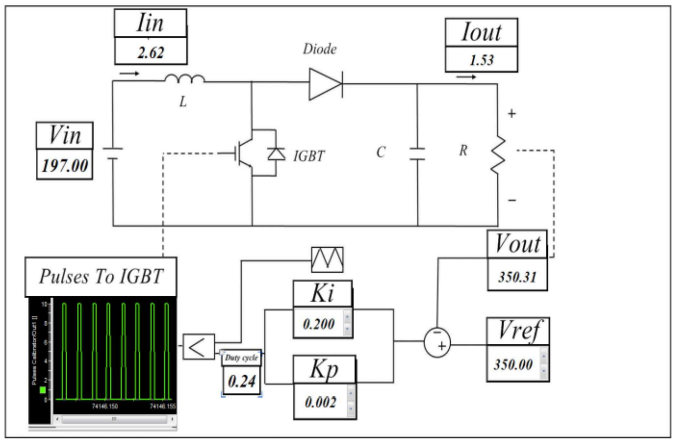

Fig. 5. Boost converter controller interface on dSPACE.

The DC-DC converter was tested and validated by fixing the output voltage to 350 V through different PI feedback controllers implemented in the dSPACE RTI 1104 platform as shown in Fig. 5. An input voltage of 200 V was supplied from the DC programmable power supply. Fig. 6 shows the response when K_p and K_i were set up to be 0.002 and 0.2, respectively. The desired voltage was changed in steps between 250 and 350 V to test the robustness of the controller. It can be seen that the response has a slight over shoot with short rise time in the red circle because of the relatively high K_i. In addition, the ripples in the input current decreased when V_{ref} was 250 V because the duty cycle decreased. V_{in} starts to encounter ripples once the switching starts because of the input resistance of the programmable power supply.

Fig. 7 shows the response for the same reference voltage variations but with smaller K_i. It can be noticed that the response became smoother with longer rise time. It is worth mentioning that the limits of the measurement devices must be taken into consideration while designing the controller, since it might lead to controller failure if they saturate leading to high input current. It is recommended to use saturation limits on the duty cycle for protection.

B. Bidirectional DC/DC converter

To interface the battery system, a bidirectional DC-DC converter (BDC), as shown in Fig. 8, was designed to charge/discharge the batteries, targeting low current ripple in order to achieve higher efficiency and longer life time. The following equations were used, along with (1) and (2) to select the values of the filters.

$$\Delta I_{HV\ side} = \frac{V_{in}\ D}{f\ L} \tag{3}$$

$$\Delta V_{HV\ side} = \frac{I_{out}\ D}{f\ C} \tag{4}$$

$$\Delta I_{LV\ side} = \frac{V_{out}(V_{in} - V_{out})\ D}{f\ L\ V_{in}} \tag{5}$$

$$\Delta V_{LV\ side} = \frac{V_{in}\ D(1-D)}{8\ L\ C\ f^2} \tag{6}$$

Where, (3) and (4) show the inductor current and capacitor voltage ripples, respectively, for the boost side and (5) and (6) show the inductor current and capacitor voltage ripples, respectively, for the buck side.

The DC-DC bidirectional converter was tested and validated by controlling the current in both directions. The battery side was emulated with a DC source in parallel with a 75-ohms resistor set to 250 V, and the DC bus side was set to 400 V with a 100 ohms DC load in parallel as shown in Fig. 8.

Fig. 9 shows the charging case when the bidirectional controller was commanded to charge by setting I_{ref} to 3 A (buck mode), while in Fig. 10 shows the discharging case where I_{ref} is set to -2 A (boost mode). It can be noticed that the controller was set up to automatically detect the required mode of operation, buck or boost, based on the sign of I_{ref}.

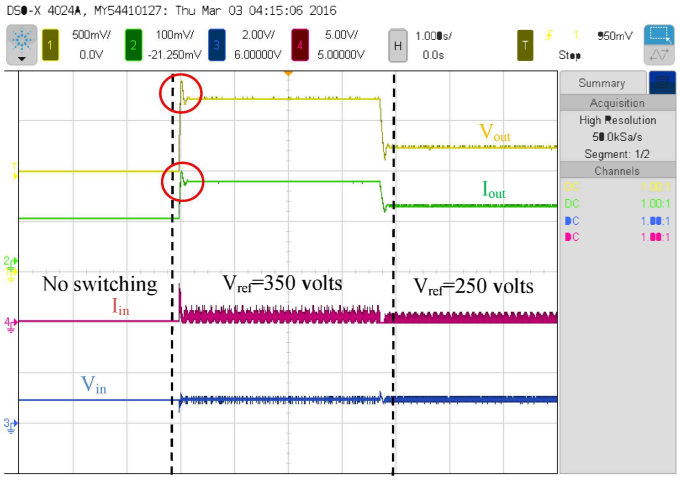

Fig. 6. Response of boost converter with K_p= 0.002 and K_i= 0.2.

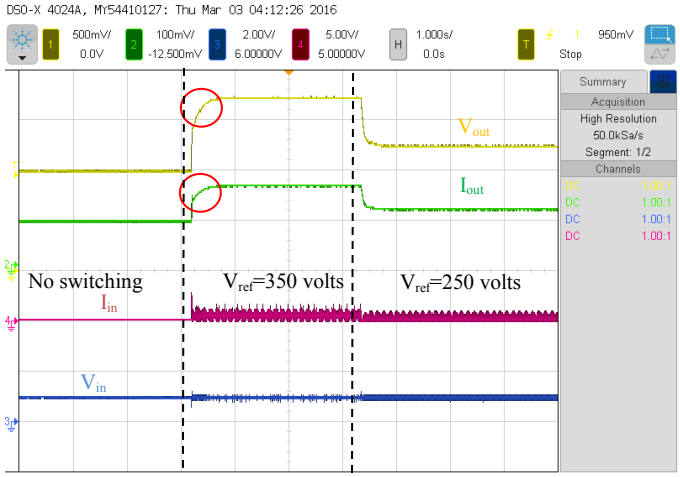

Fig. 7. Response of boost converter with K_p= 0.002 and K_i= 0.02.

C. Inverter circuit

One of the key features of the DC microgrid is to be able to inject/receive power from the grid based on the generation and loading conditions. In order to achieve this, the inverter along with the interface circuit (CTs, VTs, filters and SSR) were implemented and tested. The value of the AC inductor filter was chosen to improve the current waveform. A too large filter may result in limiting the power transfer capability, corresponding to the simplified equation, assuming the sinusoidal pulse width modulation converter can be modeled with a current source behind filter reactance.

$$P_{MG} = \frac{V_{INV}\ V_G}{X} \sin\delta \tag{7}$$

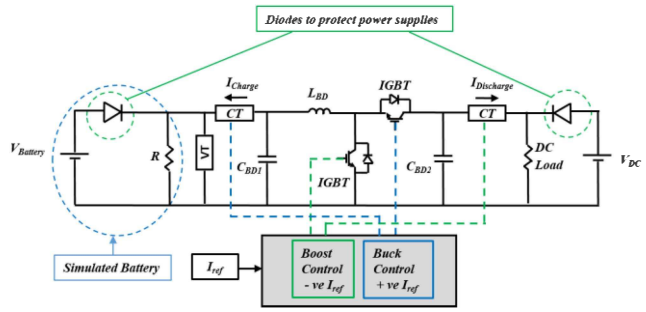

Fig. 8. Bidirectional converter testing circuit diagram.

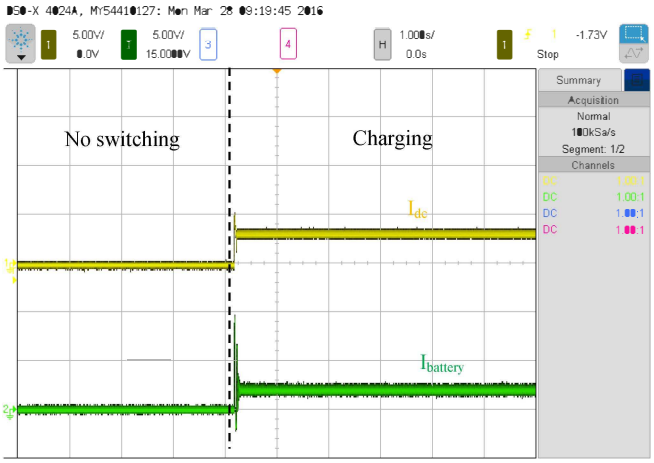

Fig. 9. Bidirectional converter response during charging.

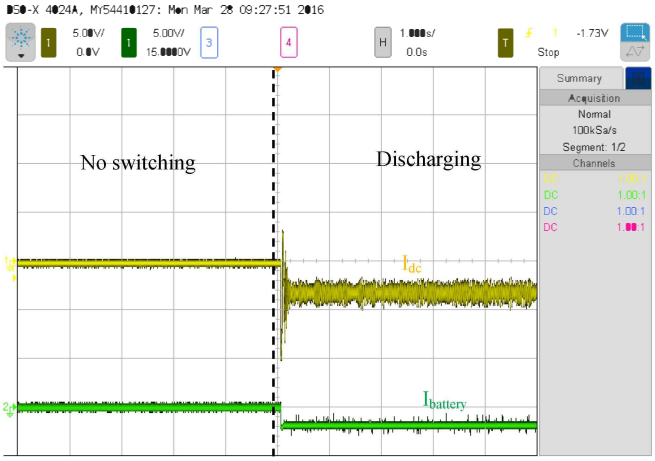

Fig. 10. Bidirectional converter response during discharging.

Where P_{MG} is the power transferred between the microgrid and the main grid, V_{INV} and V_G are the voltages at the inverter and the grid and δ is the phase difference.

In order to overcome the limit on the power transfer, the DC bus voltage can be flexibly increased.

Fig. 11 shows the circuit used for testing. Fig. 12 shows the inverter operated in the current control mode. The control decouple the active (P) and reactive (Q) power. I_d corresponds to P, and I_q corresponds to Q. It was commanded to send 3 A to the legacy grid by having a step change in I_d from 0 to 3 A. It can be seen that when I_d increased, i_a increased and that it is in phase with v_a. Fig. 13 shows when the inverter is operated at a unity power factor, it was commanded to send active power to the utility grid by setting I_d to 3 A and suddenly reversing the direction of the current by setting I_d to -3 A. It can be noticed that i_a and v_a were in phase, and then when the current reverse its direction, i_a and v_a became 180° phase shifted.

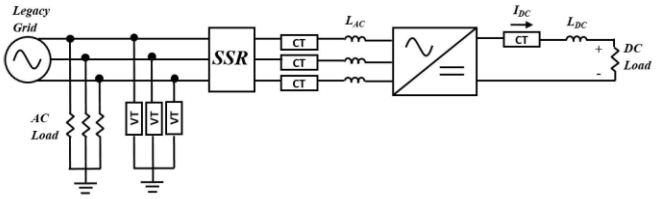

Fig. 11. Inverter testing circuit diagram.

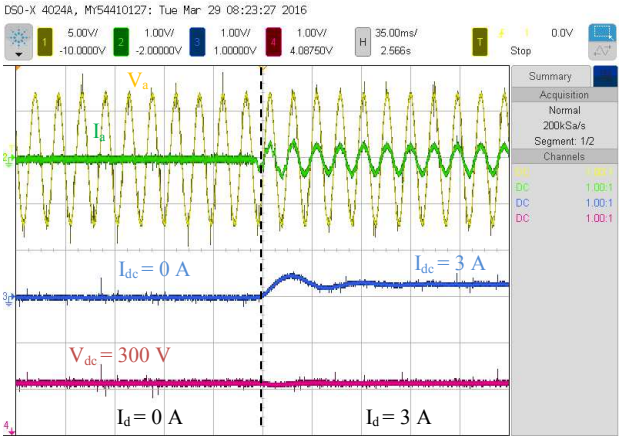

Fig. 12. Sending P to the utility grid.

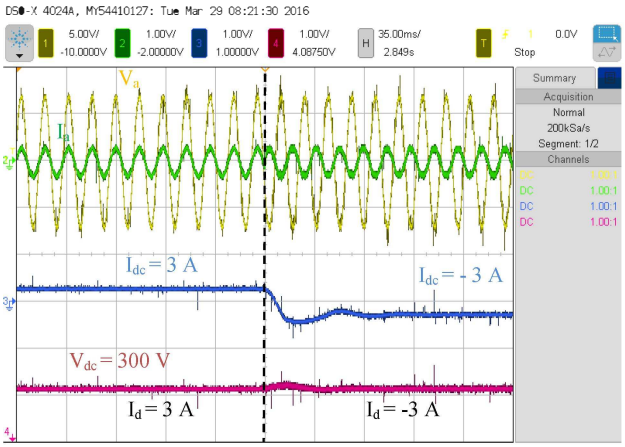

Fig. 13. Sending/receiving P to/from the utility grid.

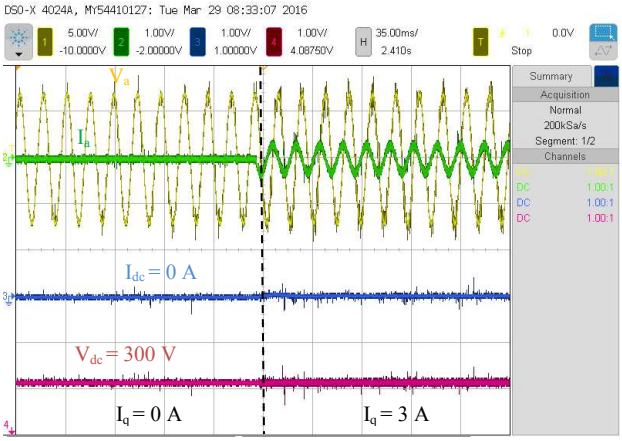

Fig. 14. Sending Q to the utility grid.

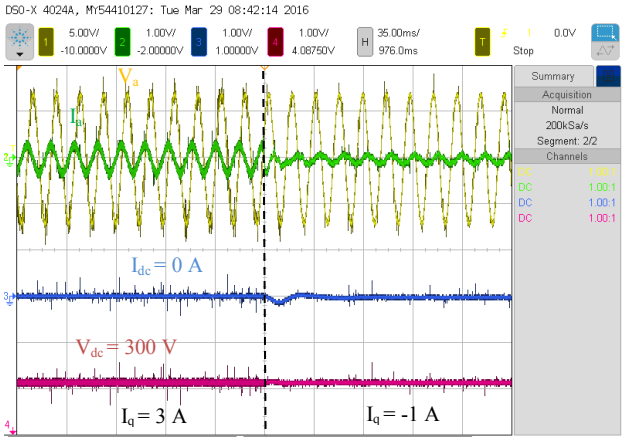

Fig. 15. Sending/receiving Q to the utility grid.

Moreover, sending and receiving Q was tested. Fig. 14 shows 90° phase shift between i_a leading v_a when the inverter controller was commanded to send Q to the utility grid by setting I_q to 3 A, which might be used to enhance the voltage level of the PCC. In Fig. 15, the inverter controller was commanded to change I_q from 3 A to -1 A, it can be noticed that i_a was leading v_a by 90° then lagged by 90°. These results show the ability of the inverter to instantly reverse the mode of sending or receiving active/reactive power.

V. Experimental Results and Discussion

The fully controlled inverter used, was operated at a switching frequency of 6.06 kHz and a sampling time of 0.1 ms for the digital controller, which allows quick responses when the desired values for P and Q are changed through I_d and I_q. Two experiments were performed to examine the performance of the microgrid under different operational scenarios.

A. Experiment 1

In this case, the inverter is commanded to send active power to the utility grid to simulate peak shaving during demand response events. In this experiment, the DC bus voltage was regulated via the boost converter while the battery charger and the grid inverter are free to send or receive power. Fig. 16 illustrates the results of this case. Two events were tested within the same experiment: 1) the grid inverter draws 0.9 kW to the utility grid while the DER is fixing the DC bus voltage at 300 V through the DC-DC boost converter. When I_d is set to 3 A, the DC-DC boost converter, which acts here as a slack bus, reacts and increase its output current to maintain the voltage. 2) The bidirectional converter starts to discharge the batteries by setting $I_{bidirectional}$ to inject 4 A reducing the stress on the DER while maintaining the power delivered to the utility grid.

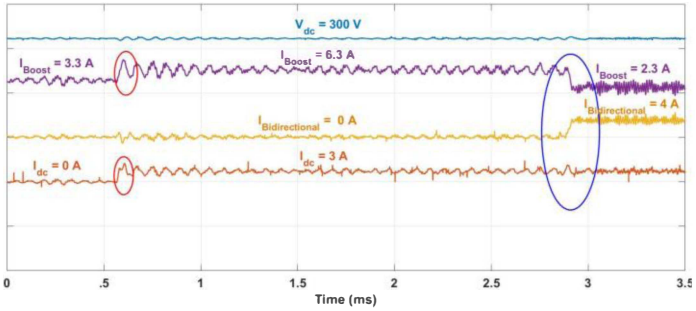

Fig. 16. Experiment 1 results.

B. Experiment 2

This experiment represents another situation when receiving active power from the grid during low energy price to share the 1.1 kW DC load with the DER, and charge the batteries. Fig. 17 shows that the inverter controller was commanded to receive 0.9 kW by setting I_d to -3 A, it can be seen that the DER reduces its current to maintain the voltage level at the DC bus to 300 V. About 1 sec later, the bidirectional converter starts to charge the batteries by setting $I_{bidirectional}$ to 2 A. It can be noticed that the DER reacts by increasing its output current through the boost converter, and the ripples increased slightly because of the interaction of both ripples from the boost and bidirectional converters.

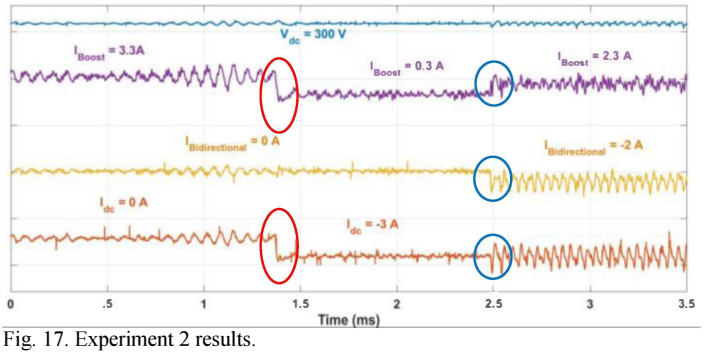

Fig. 17. Experiment 2 results.

VI. Conclusion

In order to successfully operate, maintain, and upgrade the future smart grid, it is crucial to validate research ideas experimentally along with the common simulation-based studies. This paper presented the development and implementation of a DC microgrid testbed. The design of the various power electronic converters and controllers was discussed. Various experiments were performed to validate the applicability of the individual components as well as the whole microgrid. Results showed that the implemented microgrid can be flexibly used to test various ideas related to microgrid operation and control. As a future step, the authors are currently in the process of integrating the developed hardware-based microgrid setup with a Real Time Digital Simulation system, to enable real-time HIL testing.

VII. References

[1] F. Li et al., "Smart transmission grid: Vision and framework," IEEE Trans. Smart Grid, vol. 1, no. 2, pp. 168–177, Sep. 2010.

[2] U.S. Department of Energy. (2009, Jul. 29). The Smart Grid: An Introduction [Online]. Available: http://energy.gov/oe/downloads/smartgrid-Introduction-07.

[3] Mahmoud S. Saleh, Ammar Althaibani, Yusef Esa, Yassine Mhandi, Ahmed A. Mohamed, "Impact of Clustering Microgrids on their Stability and Resilience during Blackouts," presented at Offenburg University of Applied Sciences. ICSGCE, Offenburg, Germany, 2015.

[4] "Microgrid Activities." *Microgrid Activities.* Department of Energy, n.d. Web. 28 Mar. 2016.

[5] L. Che, M. Shahidehpour, A. Alabdulwahab, "Hierarchical Coordination of a Community Microgrid With AC and DC Microgrids" IEEE Transactions on smart grid, vol. 6, no. 6, Novamber 2015.

[6] Z. Wang, B. Chen, J. Wang, C. Chen, "Networked Microgrids for Self-Healing Power Systems" IEEE Transactions on smart grid, vol. 7, no. 1, January 2016.

[7] C. Chen, J. Wang, F. Qiu, D. Zhao, "Resilient Distribution System by Microgrids Formation After Natural Disasters" IEEE Transactions on smart grid.

[8] F. Shahnia, S. Bourbour, A. Ghosh, “Coupling Neighboring Microgrids for Overload Management Based on Dynamic Multicriteria Decision-Making” IEEE Transactions on smart grid.

[9] C. Marnay, S. Chatzivasileiadis, C. Abbey, R. Iravani, G. Joos, P. Lombardi, P. Mancarella, J. Appen, “Microgrid Evolution Roadmap” International Symposium on Smart Electric Distribution Systems and Technologies, September 2015.

[10] E. Hossain, E. Kabalci, R. Bayindir, R. Perez, “Microgrid testbeds around the world: State of art”, Energy Conversion and Management, vol. 86, pp. 132-153, October 2014.

[11] Z. Liu, X. Xu, H. A. Abdelsalam, and E. Makram, "Power System Harmonics Study for Unbalanced Microgrid System with PV Sources and Nonlinear Loads," Journal of Power and Energy Engineering, vol. 3, p. 43, 2015.

[12] S. Backhaus, G. W. Swift, S. Chatzivasileiadis, W. Tschudi, S. Glover, M. Starke, J. Wang, M. Yue, and D. Hammerstrom, “DC Scoping Study—Estimate of Technical and Economic Benefit,” LA-UR-15 22097, Los Alamos National Laboratory, March 2015.

[13] H. Lotfi and A. Khodaei, “AC vs. DC Microgrid Planning,” IEEE Transactions on Smart Grids, vol. 99, no. 3, pp. 1-2 4,August. 2015.

[14] A. Bidram, A. Davoudi, "Hierarchical Structure of Microgrids Control System," IEEE, vol. 3, no. 4, p. 1963, 2012.

[15] G. Dehnavi and H. L. Ginn, “Distributed control of orthogonal current components among converters in an autonomous microgrid,” in *Proc.* IEEE Energy Convers. Congr. Expo. (ECCE), Raleigh, NC, USA, 2012, pp. 974–981.

[16] A. Bidram, A. Davoudi, F. L. Lewis, and J. M. Guerrero, “Distributed cooperative secondary control of microgrids using feedback linearization” *IEEE Trans. Power Syst.*, vol. 28, no. 3, pp. 3462–3470, Aug. 2013.

[17] B. Xiao, M. Starke, G. Liu, B. Ollis, P. Irminger, A. Dimitrovski, K. Prabakar, K. Dowling, Y. Xu, “Development of Hardware-in-the-loop Microgrid Testbed” ECCE, Montereal., QC, 2015, PP. 1196-1199.

[18] R. Lasseter, J. Eto, B. Schenkman, J. Stevens, H. Vollkommer, D. Klapp, E. Linton, H. Hurtado, J. Roy, “CERTS Microgrid Laboratory Test Bed” IEEE TRANSACTIONS ON POWER DELIVERY, VOL. 26, NO. 1, JANUARY 2011.

[19] G. Turner, J. Kelley, C. Storm, D. Wetz, W. Lee, “Design and Active Control of a Microgrid Testbed” IEEE Transactions on Smart Grid, VOL. 6, NO. 1, JANUARY 2015.

[20] A. Mohamed, M. Elshaer, O. Mohammed, “Bi-Directional AC-DC/DC-AC Converter for Power Sharing of Hybrid AC/DC Systems” *in Proc. of IEEE PES General Meeting 2011, Detroit, Michigan, USA, July 24-28, 2011.*

[21] M.Milosevic, "Decoupling Control of d and q Current Components in Three-Phase Voltage Source Inverter", ETHZ, 1999.

[22] Aluminum Electrolytic Capacitors Data Manual, Vishay Americas Inc., Malvern, PA, 2012.

[23] M. H. Rashid, Power Electronics, Third edition, pp. 187-195, 2003.

[24] A. Kwasinski “Power Electronics, DC-DC Boost Converter”. EE462L Lab., Univ. Texas, Austin, Feb. 22, 2014.

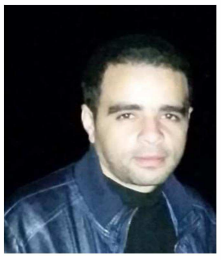

Mahmoud S. Saleh is a PhD student at the Smart Grid Laboratory, Department of Electrical Engineering, Grove School of Engineering, City collage of New York (CCNY). He received his M.S. in Electrical Engineering from CCNY in 2013. He finished his FE in 2011. His research interest includes microgrids design, control and optimization, behavior of interconnected microgrids, microgrid control hierarchy and stability.

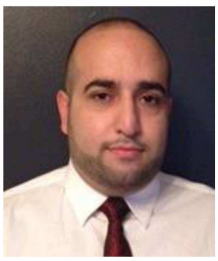

Yusef Esa is a M.S. student at the Smart Grid Laboratory, Grove School of Engineering, City Collage of New York (CCNY). He received the B.S. degree in electrical engineering from CCNY in 2015. His research interest includes microgrids design, impact of weather changes on renewable energy resources and its prediction, battery management system optimization.

Yassine Mhandi is a M.S. student at the Smart Grid Laboratory, Grove School of Engineering, City college of New York (CCNY). He received the B.S. degree in electrical engineering from CCNY in 2015. His research interest includes Microgrids design and control, mathematical modeling of interconnected microgrids, and load prediction techniques.

Werner Brandauer is a postdoctoral research fellow at the Smart Grid Laboratory, Department of Electrical Engineering at the Grove School of Engineering, City College of the City University of New York. He received his PhD degree in 2014 from Graz University of Technology. His main research interests include microgrids, power system modeling, power system economics and renewable energy systems.

Ahmed A. Mohamed (El-Tallawy) (GS’2009, M’2013) is an Assistant Professor of Electrical Engineering at the Grove School of Engineering, City College of the City University of New York (CCNY). He is the director of the Smart Grid Laboratory at CCNY. His main research interests include microgrid design and control, electric vehicles and impact of space weather on electric power systems.